Universiteit Leiden
The Netherlands

Catalytic water splitting with an iridium carbene complex: a theoretical study

Venturini, A.; Barbieri, A.; Reek, J.N.H.; Hetterscheid, D.G.H.

Citation
Venturini, A., Barbieri, A., Reek, J. N. H., & Hetterscheid, D. G. H. (2014). Catalytic water splitting with an iridium carbene complex: a theoretical study. *Chemistry: A European Journal*, *20*(18), 5358-5368. doi:10.1002/chem.201303796

Version: Publisher's Version
License: Licensed under Article 25fa Copyright Act/Law (Amendment Taverne)
Downloaded from: https://hdl.handle.net/1887/3238683

Note: To cite this publication please use the final published version (if applicable).

ChemPubSoc Europe

DOI: 10.1002/chem.201303796

CHEMISTRY
A European Journal
Full Paper

Water Splitting

Catalytic Water Splitting with an Iridium Carbene Complex: A Theoretical Study

Alessandro Venturini,*[a] Andrea Barbieri,[a] Joost N. H. Reek,[b] and Dennis G. H. Hetterscheid*[c]

Abstract: Catalytic water oxidation at $\mathbf{Ir}(OH)^+$ ($\mathbf{Ir}$ = IrCp*-(Me_2NHC), where Cp* = pentamethylcyclopentadienyl and Me_2NHC = *N*,*N*′-dimethylimidazolin-2-ylidene) can occur through various competing channels. A potential-energy surface showing these various multichannel reaction pathways provides a picture of how their importance can be influenced by changes in the oxidant potential. In the most favourable calculated mechanism, water oxidation occurs via a pathway that includes four sequential oxidation steps, prior to formation of the O–O bond. The first three oxidation steps are exothermic upon treatment with cerium ammonium nitrate and lead to formation of $\mathbf{Ir}^V(=O)(O^\bullet)^+$, which is calculated to be the most stabile species under these conditions, whereas the fourth oxidation step is the potential-energy-determining step. O–O bond formation takes place by coupling of the two oxo ligands along a direct pathway in the rate-limiting step. Dissociation of dioxygen occurs in two sequential steps, regenerating the starting material $\mathbf{Ir}(OH)^+$. The calculated mechanism fits well with the experimentally observed rate law: $v = k_{obs}[\mathbf{Ir}][\text{oxidant}]$. The calculated effective barrier of 24.6 kcal mol^{-1} fits well with the observed turnover frequency of 0.88 s^{-1}. Under strongly oxidative conditions, O–O bond formation after four sequential oxidation steps is the preferred pathway, whereas under milder conditions O–O bond formation after three sequential oxidation steps becomes competitive.

Introduction

To mimic nature, which fulfils its energy requirements through photosynthesis by using sunlight and water to convert carbon dioxide to carbohydrates, scientists have developed artificial water-splitting systems in order to find solutions to the increasing demand for energy.[1] Fundamental understanding of how water oxidation can occur efficiently is a major knowledge gap that must be overcome in order to produce chemical fuels from solar energy. This is important in becoming independent of fossil fuels.[2] Since the discovery of the ruthenium blue dimer by Meyer and co-workers in the 1980s,[3] and especially after the publication of the first mononuclear water-oxidation catalysts at the beginning of this century,[4] the number of publications has exploded. Besides many heterogeneous systems,[5] molecular manganese-,[6] iron-,[7] cobalt-[8] and copper-based[9] systems have been published. Especially ruthenium catalysts have gained much attention.[4e–g,10] Detailed studies on several systems have led to great understanding of the catalytic mechanism by which these complexes operate. This has also led to very active ruthenium systems that now can operate with turnover frequencies similar to those of the manganese oxo cluster of photosystem II.[11] Molecular iridium catalysts for water oxidation have received less attention than their ruthenium counterparts, and the mechanism by which they operate is less clear. The first molecular iridium water-oxidation catalyst, which was reported by Bernhard et al., showed only moderate O_2 evolution rates upon addition of cerium ammonium nitrate (CAN), a strong stoichiometric oxidant that is typically used to study water oxidation.[12] Crabtree and co-workers introduced pentamethylcyclopentadienyl (Cp*) ligands for iridium-based water-oxidation catalysts,[13] and although the stability of these ligands is not always clear,[14] highly active water-oxidation systems have been reported by several groups. Water oxidation was shown to proceed via molecular active species in the initial stage of the catalytic reaction for at least some of these catalysts.[15] Water oxidation mediated by these catalysts was proposed to proceed via iridium(V) intermediates. Recent studies showed that for some complexes the Cp* ligand can be lost easily and that part of the catalytic activity must be ascribed to the product of Cp* release rather than the intact precursor.[16] Contradicting studies show that Cp* can be retained, even during long-term electrolysis.[17] In 2011 we demonstrated that $[IrCp^*(Me_2NHC)(OH)_2]$ (Me_2NHC = *N*,*N*′-dimethylimidazolin-

[a] Dr. A. Venturini, Dr. A. Barbieri
Institute for the Organic Synthesis and Photoreactivity
National Research Council of Italy
Via P. Gobetti 101, 40129 Bologna (Italy)
E-mail: alessandro.venturini@isof.cnr.it

[b] Prof. Dr. J. N. H. Reek
Van't Hoff Institute for Molecular Sciences
University of Amsterdam
Sciencepark 904, Amsterdam (The Netherlands)

[c] Dr. D. G. H. Hetterscheid
Leiden Institute of Chemistry, Leiden University
Einsteinweg 55, Leiden (The Netherlands)
E-mail: d.g.h.hetterscheid@chem.leidenuniv.nl

Supporting information for this article is available on the WWW under http://dx.doi.org/10.1002/chem.201303796.

© 2014 Wiley-VCH Verlag GmbH & Co. KGaA, Weinheim

2-ylidene) is a water-oxidation catalyst.[18] We anticipated that the strongly electron donating *N*-heterocyclic carbene (NHC) ligand would make the +V oxidation state more easily accessible, and indeed we obtained excellent turnover frequencies compared to other iridium systems.[18,19] In contrast to these other iridium Cp* complexes, $[IrCp^*(Me_2NHC)(OH)_2]$ has two vacant sites at which oxidation of water can occur, and this allows for different oxidation pathways that are not accessible to iridium catalysts that do not have a second free site. The main advantage is that higher oxidation states may be accessible through proton-coupled electron transfer (PCET) leading to more reactive iridium oxo species without unfavourable uncoupled oxidation events, which by definition take place at high overpotential. In analogy to this, it was shown for the mononuclear catalyst $[Ru(bpy)_2(OH_2)_2]^{2+}$ (bpy = 2,2′-bipyridine) that the ruthenium centre cycles from the +II all the way to the +VI oxidation state prior to formation of the O–O bond.[20]

In the present work, we studied the mechanism of water oxidation mediated by $[IrCp^*(Me_2NHC)(OH)_2]$ by means of DFT calculations. Our aim was to give an accurate description of the potential-energy surface (PES) of the water-oxidation reaction [Equation (1)] mediated by $[IrCp^*(Me_2NHC)(OH)_2]$. This is a difficult task for this kind of reaction, due to the complexity and in particular to the presence of mechanistic steps of different nature.

$$2\,H_2O \rightarrow O_2 + 4\,H^+ + 4\,e^- \quad (1)$$

Four electrons and four protons are removed from two water molecules, and an O–O bond is formed. The reaction occurs under acidic conditions and the most important intermediates have single positive charges. Following the mechanistic evolution of the system with a single positive charge, we take into account all possible mechanistic steps: PCET, one-electron transfers, formation of O–O bonds and reversible coordination of additional water molecules. We demonstrate that high-valent iridium complexes with formal oxidation states of +VI and +VII are accessible under strongly oxidative conditions and result in rapid O–O bond formation. Moreover, we show that the $[IrCp^*(Me_2NHC)(OH)_2]$ precursor itself can be the active species in water oxidation. The proposed mechanism agrees well with the experimental data obtained by kinetic studies through initial rates[19] and in situ mass spectrometry experiments,[18] although the different conditions used for mass spectrometric detection compared to the reaction did not allow detection of species with higher oxidation states.[21]

Results and Discussion

The whole potential-energy surface (PES) is a combination of different mechanistic steps. These include PCET steps, coordination and elimination of water, formation of the O–O bond and dissociation of dioxygen from the complex. All these steps can proceed at different stages of the catalytic cycle and may be in competition with each other. First, we analyse the individual steps separately before combining them to describe the entire PES. Since monocationic species were observed by ESI-MS, we calculated the PES only for singly charged catalytic species. This does not rule out that part of the catalytic cycle may proceed via species with a different charge. Therefore, dicationic species were also considered. Since the experimental data were obtained under strongly protic conditions (between pH 0 and 1), neutral intermediates were not investigated.

To simplify the discussion, $IrCp^*(Me_2NHC)$ is abbreviated to **Ir** and only O_2 and the oxygen-based ligands such as (partly) oxidized water are depicted. The oxidation state is given according to the Mulliken spin-density population, but is not always meaningful in the case of the species with higher oxidation states. The total energies of the intermediates are given in Table S1 of the Supporting Information, and an overview of all reactions and species considered in this work is depicted in Figure 1. The mechanism can be described in columns with vertical and rows with horizontal arrows. Vertical arrows are PCET steps, whereas horizontal arrows correspond to equilibria in which the complex gains or loses a water ligand. The circular arrows marked with "O–O" represent O–O bond formation. The predominant species observed experimentally by ESI-MS, that is, $\mathbf{Ir}^{III}(OH)^+$, $\mathbf{Ir}^{IV}(=O)^+$ and $\mathbf{Ir}^{V}(OH)_3{}^+$, are involved in O_2 formation along the various pathways considered here.[18]

Proton-coupled electron transfer

To take the PCET steps into account we used isodesmic equations to calculate the stabilization energy (SE) [Eq. (2)]

$$SE = [E1(X) + E2(Y)] - [E2(X) + E1(Y)] \quad (2)$$

where E1(X), E2(X), E1(Y) and E2(Y) are the total energies obtained from the DFT calculations. Using these isodesmic equations, we can compare the energy that is required for a PCET reaction between two catalytic intermediates to that of a standard PCET reaction within the catalytic cycle. For this purpose, the oxidation of $\mathbf{Ir}^{III}(OH)^+$ to $\mathbf{Ir}^{IV}(=O)^+$ was chosen as reference. Hence, E1(Y) represents the energy of the starting material of the PCET reaction, E2(Y) the energy of the product of the PCET reaction, E1(X) the energy of $\mathbf{Ir}^{III}(OH)^+$ and E2(X) the energy of $\mathbf{Ir}^{IV}(=O)^+$. These equations offer the advantage that the number of spins, charges and atoms is kept constant on both sides of the equation and therefore allow the energies to be compared with maximum cancellation of errors. Equation (2) allows us to compare the stabilization energy upon a PCET reaction with that of the oxidation of $\mathbf{Ir}^{III}(OH)^+$ to $\mathbf{Ir}^{IV}(=O)^+$. A positive value of SE indicates that the PCET step is thermodynamically favoured in comparison with the reference reaction, whereas a negative value indicates that oxidation and loss of a proton are more difficult than oxidation of $\mathbf{Ir}^{III}(OH)^+$ to $\mathbf{Ir}^{IV}(=O)^+$.

The relative SE values show that PCET reactions in which the proton originates from an aqua ligand are relatively easy and occur at lower potentials compared to the $\mathbf{Ir}^{III}(OH)^+/\mathbf{Ir}^{IV}(=O)^+$ couple. PCET reactions in which the proton originates from a hydroxo ligand are significantly more difficult, because these events produce terminal iridium oxo species. Group 7 and 8

© 2014 Wiley-VCH Verlag GmbH & Co. KGaA, Weinheim

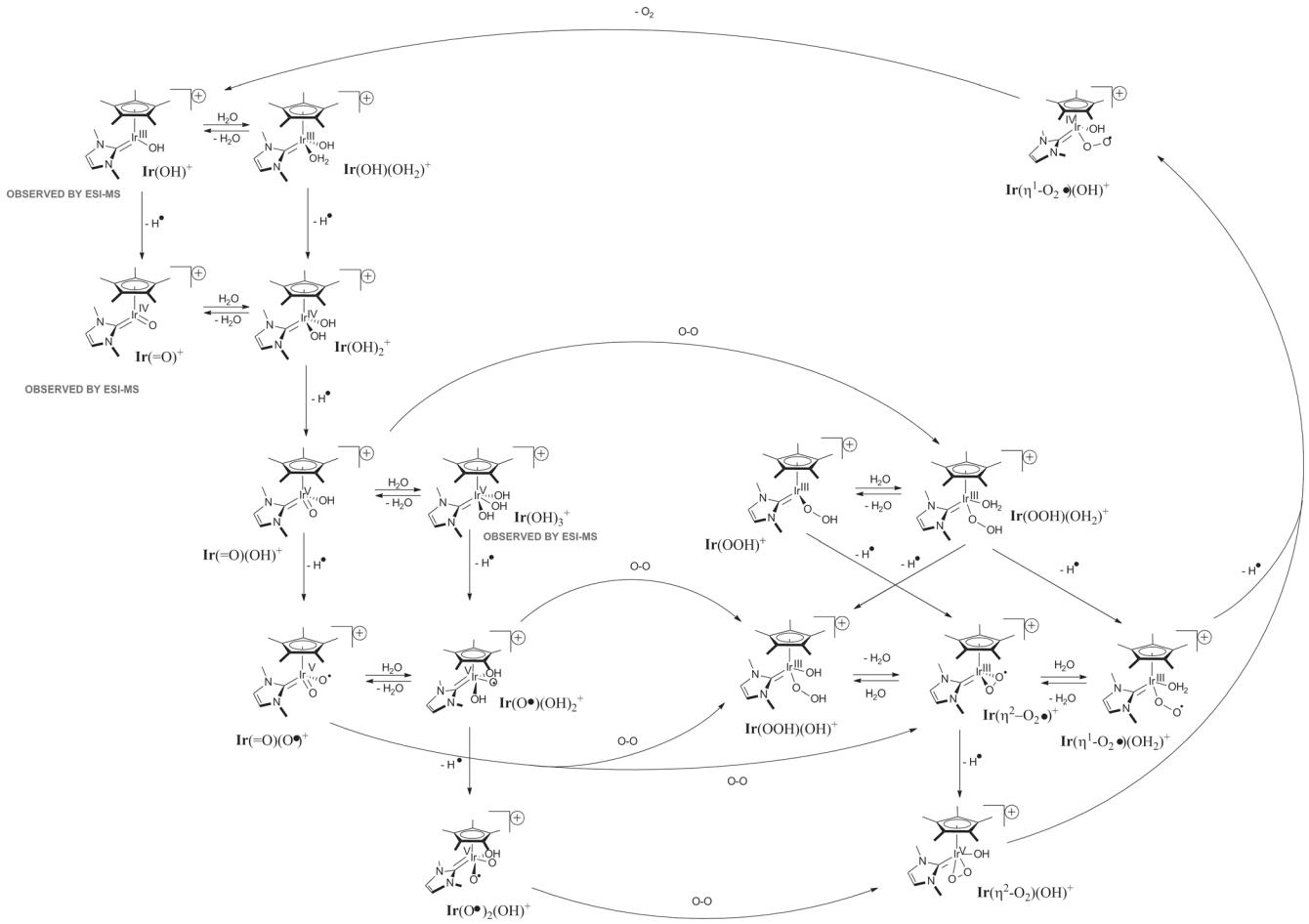

Figure 1. Catalytic intermediates investigated in this work. Water oxidation occurs by four PCET reactions, two additions of water, O–O bond formation and displacement of O_2 by H_2O. Individual reactions are shown in Schemes 1–6 and Figure 4. For all O–O bond-formation reactions the dicationic species were also calculated.

metal oxo species are typically unstable, as metal oxo antibonding orbitals are populated, and consequently very few stable iridium and platinum oxo species have been reported.[22] Once the first oxo moiety has formed, formation of the second oxo ligand is remarkably exergonic and leads to stable $\mathbf{Ir}^{V}(=O)(O^{\bullet})^{+}$. This intermediate has a stabilizing mesomeric effect due to delocalization of the uncoupled electron and the double bond between the O and Ir atoms. Calculated Mulliken spin densities are 0.33, 0.34 and 0.35 for the two O and Ir atoms respectively, whereas the bond orders are 1.62 and 1.61 (see Figure 2).

All oxidation reactions following O–O bond formation were found to be relatively easy compared to oxidation of $\mathbf{Ir}^{III}(OH)^{+}$ to $\mathbf{Ir}^{IV}(=O)^{+}$. Since these reactions are quite exergonic, this implies that the preceding O–O bond-formation steps must be relatively endergonic. This especially holds for the product of O–O bond formation at an early stage of the catalytic cycle, since this is followed by a sequence of downhill reactions.

Coordination of water

Our catalyst has vacant coordination sites that are used for coordination of water to the iridium centre. Some of the systems, like $\mathbf{Ir}^{III}(OH)(OH_2)^{+}$ or $\mathbf{Ir}^{III}(OOH)(OH_2)^{+}$, are simple adducts, whereas in $\mathbf{Ir}^{IV}(OH)_2{}^{+}$, $\mathbf{Ir}^{V}(OH)_3{}^{+}$, $\mathbf{Ir}^{V}(O^{\bullet})(OH)_2{}^{+}$ and $\mathbf{Ir}^{IV}(OOH)(OH)^{+}$ the coordinated water is transformed into more stable hydroxo ligands. For calculation of the thermodynamic stability we used Equation (3)

$$\Delta\Delta G_{298} = [\Delta G_{298}(X) + \Delta G_{298}(H_2O)] - \Delta G_{298}(Y) \quad (3)$$

where X and Y correspond to the non-coordinated and water-coordinated complex, respectively. Table 2 lists the $\Delta\Delta G_{298}$ values for water-coordination equilibrium for each pair of intermediates. Negative values indicate that coordination of water leads to a less stable species compared to X. Of the entire series only the $\mathbf{Ir}^{V}(OH)_3{}^{+}$ system is more stable than the corresponding dehydrated system.

© 2014 Wiley-VCH Verlag GmbH & Co. KGaA, Weinheim

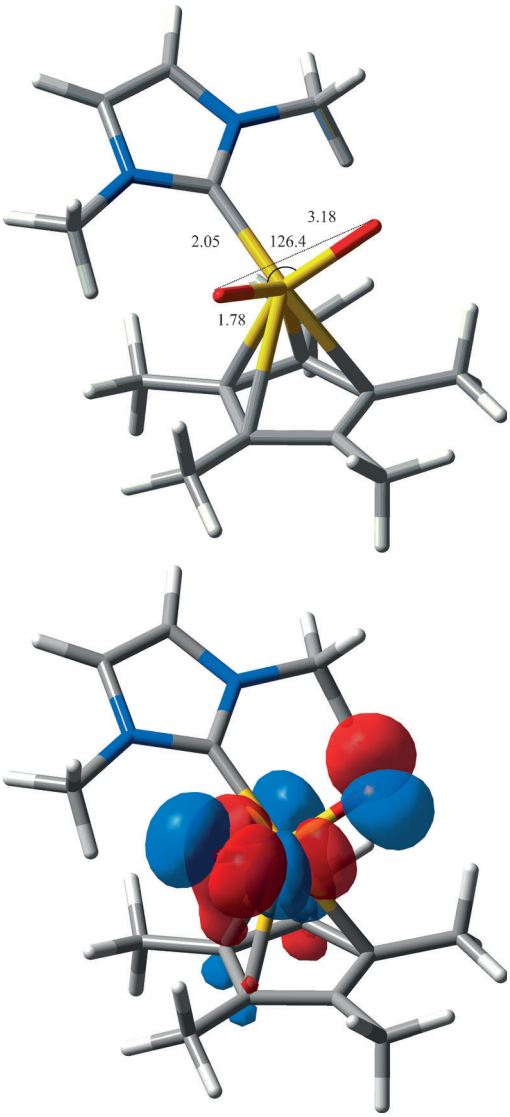

Figure 2. Optimized geometry of $Ir^{V}(O^{\bullet})(=O)^{+}$ with relevant geometrical parameters (top) and the corresponding SOMO (bottom).

O–O bond formation

Similar to other water-oxidation catalysts, formation of the O–O bond takes place in the rate-limiting step. In the present work, different O–O bond-formation pathways were considered for the cationic systems. Since uncoupled oxidation reactions sometimes occur prior to formation of the O–O bond,[4a,c,20a] we recalculated the O–O bond-formation pathways for dicationic systems as well.

From $Ir^{IV}(=O)^{+}$ to $Ir^{III}(OOH_2)^{+}$

Although we expected O–O bond formation to take place after two, three or four oxidation reactions, O–O bond formation was also considered to occur at $Ir^{IV}(=O)^{+}$. Due to the presence of only one ligand besides Me_2NHC and Cp*, $Ir^{IV}(=O)^{+}$ diverges from the typical piano-stool structure, because the O atom (Ir=O 1.8 Å) and one C atom of the Cp* group (Ir–C 2.7 Å) are in axial positions. The C atom of Me_2NHC is in equatorial position (C-Ir-O 89.7°). Although $Ir^{IV}(=O)^{+}$ can form a complex with water, we did not detect any transition state leading to formation of an O–O bond (see Scheme 1). We believe that $Ir^{IV}(=O)^{+}$ is not a strong enough electrophile to enable the reaction. Removing another electron from $Ir^{IV}(=O)^{+}$ leads to formation of $Ir^{V}(=O)^{2+}$, of which the O atom is a stronger electrophile due to the attractive force of the dicationic Ir^{V} centre. This becomes clear from the Ir=O bond lengths of 1.79 Å for the cationic Ir^{IV} species and 1.71 Å for the dicationic species. A transition state was found for nucleophilic attack of water on the dicationic system, albeit with a very high barrier of 59.8 kcal mol^{-1}.

From $Ir^{IV}(=O)(OH)^{+}$ to $Ir^{III}(OOH)(OH_2)^{+}$

Formation of the O–O bond has been described for several other iridium catalysts to occur at Ir^{V} oxo species through nucleophilic attack of water.[13a,20b] $Ir^{V}(=O)(OH)^{+}$ has a piano-stool structure in which the Ir center is bound to one oxo ligand (Ir=O 1.79 Å) and one hydroxo ligand (Ir–OH 2.03 Å) and the O-Ir-O angle is 81.2°. Addition of one water molecule to $Ir^{V}(=O)(OH)^{+}$ destabilizes it by 2.0 kcal mol^{-1}. This water adduct is the starting complex for formation of the O–O bond by nucleophilic attack of the water molecule on the iridium oxo species (Scheme 2). Figure 3 A shows the transition-state geometry, in which one of the protons of the water molecule forms a hydrogen bond with the iridium-coordinated hydroxo ligand with an HO···H distance of 1.40 Å. Simultaneously with relocation of the proton from the water molecule to the hxdroxo ligand, formation of the O–O bond takes place. For the transition state an O–O distance of 1.82 Å and an energy barrier of 30.4 kcal mol^{-1} were found. The product $Ir^{III}(OOH)(OH_2)^{+}$ is endoergic by 10.1 kcal mol^{-1} and has a piano-stool geometry in which the Ir center has an aqua ligand with an Ir–O distance of 2.30 Å, an η^1-OOH ligand with an O–O distance of 1.44 Å and a HOO–Ir distance of 2.06 Å. Coordination of water to $Ir^{V}(=O)(OH)^{+}$ produces $Ir^{V}(OH)_3^{+}$, which is lower in energy than $Ir^{V}(=O)(OH)^{+}$ by 4.0 kcal mol^{-1}. Thus, not $Ir^{V}(=O)(OH)^{+}$ but $Ir^{V}(OH)_3^{+}$ is the calculated energy minimum prior to formation of the O–O bond at this stage of the reaction. This implies that formation of the O–O bond via $Ir^{V}(=O)(OH)^{+}$ proceeds over an even larger overall barrier. Oxidation of $Ir^{V}(=O)(OH)^{+}$ in a reaction that is not coupled to proton transfer yields the dicationic

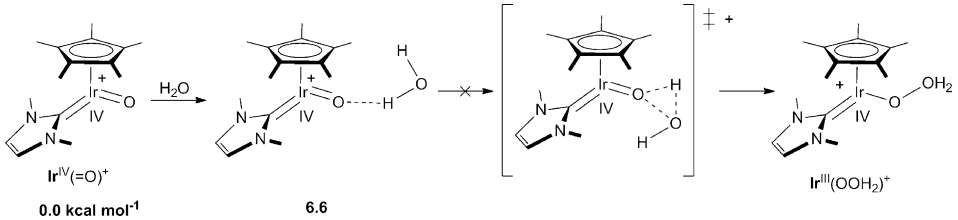

Scheme 1. Nucleophilic attack of water on $Ir^{IV}(=O)^{+}$ is difficult.

© 2014 Wiley-VCH Verlag GmbH & Co. KGaA, Weinheim

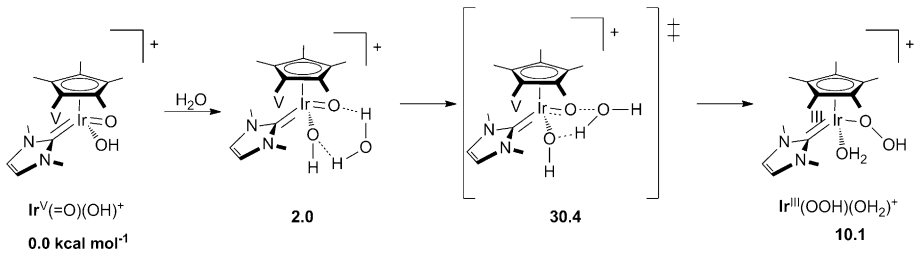

Scheme 2. Nucleophilic attack of water on $Ir^{V}(=O)(OH)^{+}$.

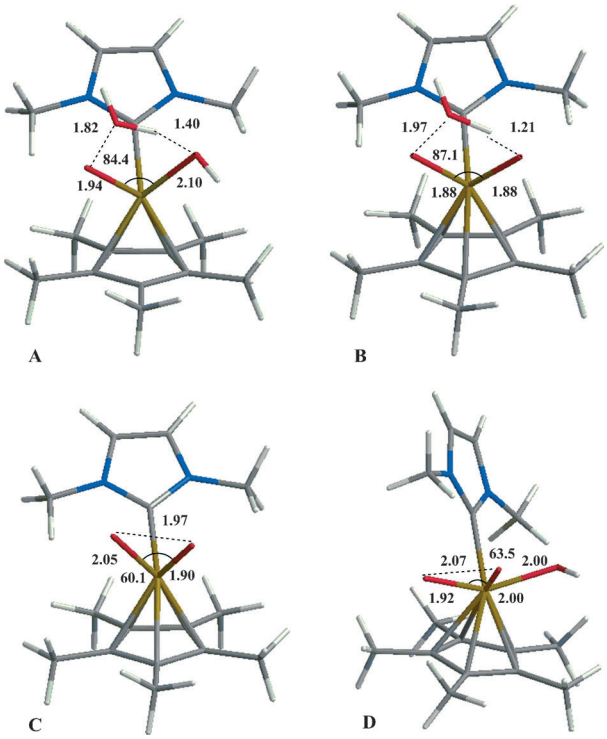

Figure 3. Transition-state geometries, with relevant geometrical parameters, for the more important O–O bond formation mechanisms. A) Addition of water to $Ir^{V}(=O)(OH)^{+}$ (Scheme 2). B) Addition of water to $Ir^{V}(=O)(O^{\bullet})^{+}$ (Scheme 3). C) Direct O–O bond formation in $Ir^{V}(=O)(O^{\bullet})^{+}$ (Scheme 4). D) Direct O–O bond formation in $Ir^{V}(OH)(O^{\bullet})_2^{+}$ (Scheme 6).

species $Ir^{VI}(=O)(OH)^{2+}$. Formation of the O–O bond starting from this intermediate leads to a barrier of 36.8 kcal mol^{-1}.

From $Ir^{V}(=O)(O^{\bullet})^{+}$ to $Ir^{IV}(OOH)(OH)^{+}$

Further oxidation of $Ir^{V}(=O)(OH)^{+}$ produces $Ir^{V}(=O)(O^{\bullet})^{+}$, which has an unpaired electron and a slightly distorted piano-stool structure. Two oxo ligands are coordinated to iridium with Ir–O bond lengths of 1.78 Å. The spin density of the unpaired electron is almost equally located on both O atoms and the iridium atom, which have radical character. Initially water forms a complex with $Ir^{V}(=O)(O^{\bullet})^{+}$ with a hydrogen-bond length of 1.90 Å. This hydrogen bond differentiates the two O atoms by making the free one more electrophilic and more prone to nucleophilic attack of water. In the transition state, the length of the forming O–O bond is 1.97 Å and the H atom is practically halfway between the two O atoms (see Figure 3B). For this transition state an energy barrier of 43.6 kcal mol^{-1} was found (Scheme 3). The product $Ir^{IV}(OOH)(OH)^{+}$ is endoergic by 13.1 kcal mol^{-1} and has a piano-stool structure with an Ir–OOH distance of 1.98 Å and an IrO–OH distance of 1.41 Å. The Ir–OH distance is 2.02 Å.

From $Ir^{V}(=O)(O^{\bullet})^{+}$ to $Ir^{IV}(\eta^2\text{-}O_2)^{+}$

Instead of a nucleophilic attack of water on $Ir^{V}(=O)(O^{\bullet})^{+}$, formation of the O–O bond can proceed by an intramolecular process (Scheme 4) that is comparable to the addition of a radical to a double bond. Contraction of the O–O distance takes place from 3.18 Å in $Ir^{V}(=O)(O^{\bullet})^{+}$ to 1.98 Å in the transition state (see Figure 1c), whereas the Ir–O bond lengths change from 1.89 to 2.05 Å, which is in agreement with a decreased Ir–O bond order and a lower oxidation state of iridium. An energy barrier of 33.4 kcal mol^{-1} was found. The product $Ir^{IV}(\eta^2\text{-}O_2)^{+}$ is exoergic by 2.1 kcal mol^{-1} and has a piano-stool geometry with a side-on coordinated peroxide ligand, Ir–O distances of 2.13 Å and an O–O distance of 1.31 Å. $Ir^{V}(=O)(O^{\bullet})^{+}$ is not the first bis-oxo species that was considered to take part in a water-oxidation mechanism. Water-oxidation activity has been ascribed to *cis*-$[Ru^{II}(bpy)_2(H_2O)_2]^{2+}$ in the past, whereby both nucleophilic attack of water and intramolecular O–O bond formation were considered.[20a] For the formal ruthenium(VI) bis-oxo intermediate, it was found that nucleophilic attack of water was the most favourable mechanism, whereas intramolecular O–O bond formation proceeds via a huge energy barrier. For $Ir^{V}(=O)(O^{\bullet})^{+}$ we found the opposite trend, and intramolecular formation of the O–O bond is the prevailing pathway. This suggests that the oxo ligands of the iridium complex are less electrophilic.

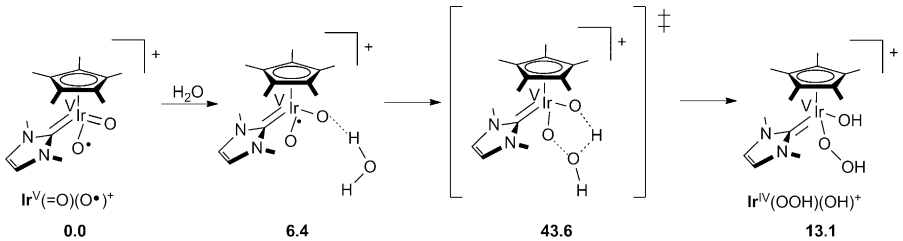

Scheme 3. Nucleophilic attack of water on $Ir^{V}(=O)(O^{\bullet})^{+}$.

© 2014 Wiley-VCH Verlag GmbH & Co. KGaA, Weinheim

Table 1. SE values of the PCET steps relative to the reference reaction $Ir^{III}(OH)^+ \rightarrow Ir^{IV}(=O)^+$.

PCET step	SE [kcal mol^{-1}]
$Ir^{III}(OH)^+$ to $Ir^{IV}(=O)^+$	0.0
$Ir^{III}(OH)(OH_2)^+$ to $Ir^{IV}(OH)_2^+$	1.4
$Ir^{IV}(OH)_2^+$ to $Ir^{V}(=O)(OH)^+$	−7.9
$Ir^{V}(=O)(OH)^+$ to $Ir^{V}(=O)(O^{\bullet})^+$	7.4
$Ir^{V}(OH)_3^+$ to $Ir^{V}(O^{\bullet})(OH)_2^+$	−9.6
$Ir^{V}(O^{\bullet})(OH)_2^+$ to $Ir^{V}(O^{\bullet})_2(OH)^+$	−14.5
$Ir^{III}(OOH)^+$ to $Ir^{IV}(\eta^2\text{-}O_2)^+$	9.5
$Ir^{III}(OOH)(OH_2)^+$ to $Ir^{IV}(OOH)(OH)^+$	4.3
$Ir^{III}(OOH)(OH_2)^+$ to $Ir^{IV}(OO^{\bullet})(OH_2)^+$	14.1
$Ir^{IV}(OOH)(OH)^+$ to $Ir^{V}(\eta^2\text{-}O_2)(OH)^+$	10.1
$Ir^{IV}(OO^{\bullet})(OH_2)^+$ to $Ir^{V}(OO^{\bullet})(OH)^+$	−0.3

Table 2. Water-equilibrium free energies $\Delta\Delta G_{298}$ [kcal mol^{-1}] calculated for X and its water adduct.

X	Y	$\Delta\Delta G_{298}$
$Ir^{III}(OH)^+$	$Ir^{III}(OH)(OH_2)^+$	−10.0
$Ir^{IV}(=O)^+$	$Ir^{IV}(OH)_2^+$	−8.6
$Ir^{V}(=O)(OH)^+$	$Ir^{V}(OH)_3^+$	4.0
$Ir^{V}(=O)(O^{\bullet})^+$	$Ir^{V}(OH)_2(O^{\bullet})^+$	−12.9
$Ir^{III}(OOH)^+$	$Ir^{III}(OOH)(OH_2)^+$	−10.1
$Ir^{IV}(\eta^2\text{-}O_2)^+$	$Ir^{IV}(OOH)(OH)^+$	−15.1
$Ir^{IV}(\eta^2\text{-}O_2)^+$	$Ir^{IV}(OO^{\bullet})^+(OH_2)^+$	−5.5

From $Ir^{V}(O^{\bullet})(OH)_2^+$ to $Ir^{IV}(OOH)(OH)^+$

The complex $\mathbf{Ir}^{V}(O^{\bullet})(OH)_2^+$ has a piano-stool geometry with four legs. It is the product of a proton-coupled oxidation reaction of the stable intermediate $\mathbf{Ir}^{V}(OH)_3^+$ or addition of water to $\mathbf{Ir}^{V}(=O)(O^{\bullet})^+$. This structure is thermodynamically unstable, as suggested by the isodesmic equation (see Table 1). The Ir–OH bond lengths are 2.0 Å and the Ir–$O^{\bullet}$ distance is 1.9 Å. The initial water complex has a hydrogen-bond length of 1.9 Å and is less stable than $\mathbf{Ir}^{V}(O^{\bullet})(OH)_2^+$ by 4.9 kcal mol^{-1}. Nucleophilic attack of water on this species proceeds via a high barrier of 50.1 kcal mol^{-1} and the product $\mathbf{Ir}^{IV}(OOH)(OH)^+$ is endoergic by 0.2 kcal mol^{-1}. In the transition state, in which formation of the O–O bond and proton transfer from the incoming water molecule to a hydroxyl ligand occur in a concerted manner, the proton has almost completely transferred to one of the two hydroxo ligands. For the transition state we found an O–O distance of 1.84 Å (Scheme 5).

From $Ir^{V}(O^{\bullet})_2(OH)^+$ to $Ir^{IV}(\eta^2\text{-}O_2)(OH)^+$

The structure of $\mathbf{Ir}^{V}(O^{\bullet})_2(OH)^+$ is very distorted. The Ir–O bond lengths are 1.76 and 1.80 Å, and the formal oxidation state of iridium in this species is +VII. Mulliken spin-population analysis suggested that it is better described as an Ir^{V} species with two coordinated oxy radicals. Complex $\mathbf{Ir}^{V}(O^{\bullet})_2(OH)^+$ is not a very stable species, and from $\mathbf{Ir}^{V}(O^{\bullet})(=O)^+$ to $\mathbf{Ir}^{V}(O^{\bullet})_2(OH)^+$ addition of water takes place in a reaction that is endergonic by 12.9 kcal mol^{-1} and a PCET reaction which is 14.5 kcal mol^{-1} higher than the reference $\mathbf{Ir}^{III}(OH)^+/\mathbf{Ir}^{IV}(=O)^+$ couple. However, we did find a facile barrier for O–O bond formation at 9.5 kcal mol^{-1} in an intramolecular process. The O–O distance shortens from 2.92 to 2.07 Å in the transition state. The product $\mathbf{Ir}^{V}(\eta^2\text{-}O_2)(OH)^+$ is exoergic by 23.8 kcal mol^{-1} and confirms that formation of the $\mathbf{Ir}^{V}(O^{\bullet})_2(OH)^+$ species must have been relatively difficult.

O_2 release

Independent of the stage at which formation of the O–O bond takes place, $\mathbf{Ir}^{V}(\eta^2\text{-}O_2)(OH)^+$ is formed, since formation of this species from the other peroxide products by PCET reactions is energetically favoured (see Table 1). Dissociation of dioxygen from $\mathbf{Ir}^{V}(\eta^2\text{-}O_2)(OH)^+$ is relatively easy and occurs through breaking of one of the Ir–O bonds leading to $\mathbf{Ir}^{IV}(\eta^1\text{-}OO^{\bullet})(OH)^+$. Formation of this species is endergonic by 0.6 kcal mol^{-1} and proceeds over a small barrier of 10.4 kcal mol^{-1}. Elimination of O_2 from $\mathbf{Ir}^{IV}(\eta^1\text{-}OO^{\bullet})(OH)^+$ proceeds via a small energy barrier of 6.7 kcal mol^{-1}. Figure 4 shows the transition states for this process including important geometric parameters.

Evaluation of the potential-energy surface

The combination of Cp* and NHC ligands affords a very electron-rich Ir^{III} centre. The system is very flexible and consequently can stabilize the iridium centre, particularly in the higher oxidation states and in different coordination geometries. As a result of the electron-rich character of the Ir^{III} species, the Ir^{III} bis-hydroxide starting material was shown to be prone to lose a hydroxo ligand once protonated. In the present work we are

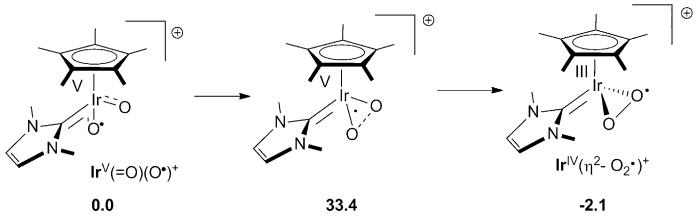

Scheme 4. Direct O–O bond formation in $\mathbf{Ir}^{V}(=O)(O^{\bullet})^+$.

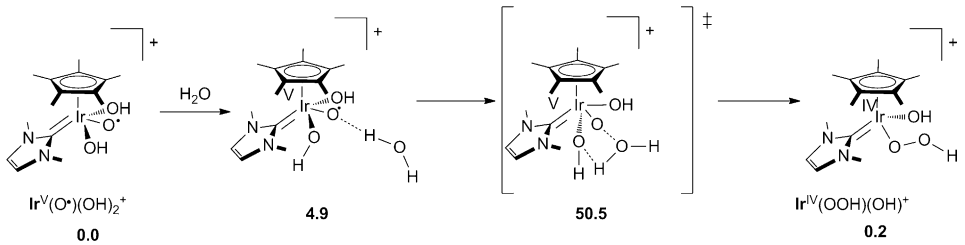

Scheme 5. Nucleophilic attack of water on $\mathbf{Ir}^{V}(OH)_2(O^{\bullet})^+$.

© 2014 Wiley-VCH Verlag GmbH & Co. KGaA, Weinheim

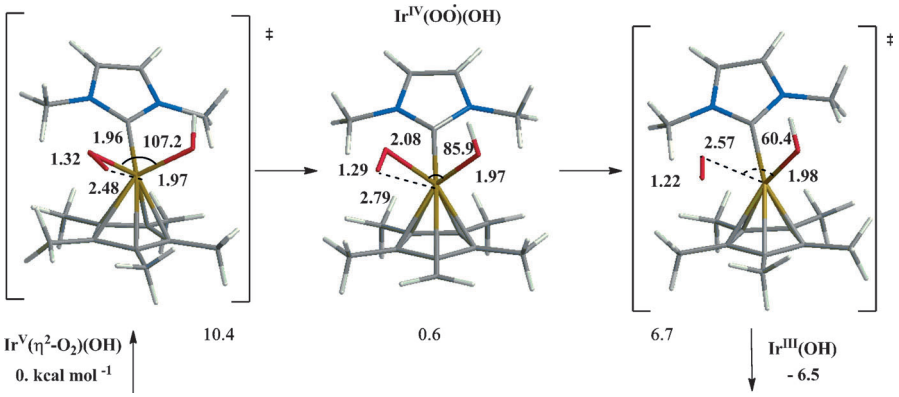

Figure 4. Geometries with relevant geometrical parameters for the O_2-release mechanism.

mainly concerned with monocationic species, because they were observed by mass spectrometry.[18] It seems unlikely that neutral species bearing hydroxo ligands are formed under the strongly acidic conditions employed upon treatment with CAN. Moreover, excellent water-oxidation catalysis was observed electrochemically at pH 1, whereas dimerization via bridging hydroxides seems to take place under strongly alkaline conditions.[19] Coordination of water upon expansion of the coordination sphere allows for additional PCET processes. In analogy with iridium Cp* catalysts bearing one vacant site for water or its (partly) oxidized intermediates, it was expected that O–O bond formation would occur by nucleophilic attack of water on the Ir^V oxo species.[13a,20b] Such O–O bond formation is also frequently encountered for many mononuclear and even dinuclear ruthenium-based water-oxidation catalysts.[4e–g,23] A barrier of 30.4 kcal mol^{-1} was found for O–O bond formation by nucleophilic attack of water on $\mathbf{Ir^V}(=O)(OH)^+$, which appears to be considerably higher than the barriers reported by Balcells et al. for [IrCp*(C^N)(OH)] and [Ir(N^C)$_2$(OH)(OH$_2$)] (N^C = cyclometallated phenylpyridine).[13a] However, the exact barrier height found may depend upon the functional that is used. Upon expansion of the coordination sphere with another aqua ligand and reshuffling of protons to form a trihydroxy system, formation of a "unstable" iridium oxo species can be avoided. Formation of the thermodynamically more favourable $\mathbf{Ir^V}(OH)_3$ species effectively lowers the concentration of $\mathbf{Ir^V}(=O)(OH)^+$. Consequently, the overall barrier for O–O bond formation is even higher. The combination of a relatively high barrier, due to the relatively electron rich Ir^{III} centre in combination with a thermodynamic sink in form of the trihydroxy species, suggests that this O–O bond-forming pathway cannot be the dominant pathway leading to evolution of O_2. Further oxidation of the Ir^V species in PCET steps results in the formation of species that formally have the metal centre in the +VI oxidation state, but are better described as the oxygen-centred radical species $\mathbf{Ir^V}(=O)(O^\bullet)^+$ and $\mathbf{Ir^V}(O^\bullet)(OH)_2^+$ (Scheme 2). In case of $\mathbf{Ir^V}(=O)(O^\bullet)^+$ the unpaired electron is delocalized on both O atoms. Hence, this species was shown to be more stable than $\mathbf{Ir^V}(O^\bullet)(OH)_2^+$ and was expected to be the starting point for easier formation of the O–O bond. Direct coupling of the two O atoms to produce the O–O bond proceeds via a barrier of 33.4 kcal mol^{-1} (Scheme 4). This reaction is significantly easier than nucleophilic attack of water on one of the oxo ligands of $\mathbf{Ir^V}(=O)(O^\bullet)^+$, whereby the other O atom acts as an internal base.

This is an entirely opposite trend to the ruthenium bis-oxo species reported by Llobet et al.[20a] Moreover, nucleophilic attack by water on $\mathbf{Ir^V}(O^\bullet)(OH)_2^+$ has a high energy barrier and is therefore unlikely (Scheme 5). In the case of [Ru(bpy)(tpy)(OH)]$^{2+}$ (tpy = terpyridine), it has been reported that water oxidation occurs by a potential-determining proton-uncoupled oxidation process leading to a more reactive metal oxo species that has a higher overall charge and is therefore more prone to nucleophilic attack by water.[4a–c] All aforementioned O–O bond-formation reactions were also tested by starting with initial dicationic structures and dicationic transition states. In none of these cases did this lead to a decrease in the transition-state energy.

Oxidation of $\mathbf{Ir^V}(O^\bullet)(OH)_2^+$ in a PCET reaction affords $\mathbf{Ir^V}(O^\bullet)_2(OH)^+$. This high-energy species, with a formal iridium oxidation state of +VII, leads to formation of the O–O bond via a low energy barrier to yield the $\mathbf{Ir^V}(\eta^2\text{-}O_2)(OH)^+$ intermediate (Scheme 6). This is an important intermediate because almost all previously discussed mechanisms proceed via its formation. The subsequent dissociation of O_2 occurs via superoxide $\mathbf{Ir^{IV}}(\eta^1\text{-}O_2^\bullet)(OH)^+$ without further coordination of water (Figure 4).

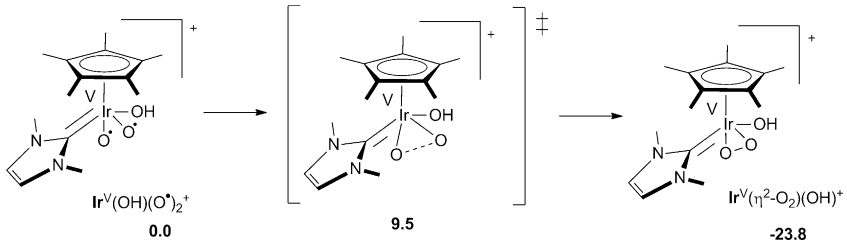

Scheme 6. Direct O–O bond formation in $\mathbf{Ir^V}(OH)(O^\bullet)_2^+$.

Although the high-valent iridium species have a lower transition state for O–O bond formation, it is important to put the relative stability of the species prior to O–O bond formation into perspective. When formation of the formally Ir^{VI} and Ir^{VII} intermediates is very endergonic, O–O bond-formation pathways

© 2014 Wiley-VCH Verlag GmbH & Co. KGaA, Weinheim

starting from these species are unlikely, regardless of the ease of this reaction. The relative energies of the PCET reactions are compared in Table 1 and correlated with the oxidation of $\mathbf{Ir}^{III}(OH)^+$ to $\mathbf{Ir}^{IV}(=O)^+$. These data show that oxidation from $\mathbf{Ir}^{III}(OH)^+$ to $\mathbf{Ir}^{IV}(=O)^+$, from $\mathbf{Ir}^{IV}(=O)^+$ to $\mathbf{Ir}^{V}(OH)^{3+}$ and from $\mathbf{Ir}^{V}(OH)_3{}^+$ to $\mathbf{Ir}^{V}(=O)(O^{\bullet})^+$ are PCET events that appear to be relatively easy in comparison with $\mathbf{Ir}^{IV}(OH)_2{}^+$ to $\mathbf{Ir}^{V}(=O)(OH)^+$, $\mathbf{Ir}^{V}(OH)_3{}^+$ to $\mathbf{Ir}^{V}(O^{\bullet})(OH)_2{}^+$ and $\mathbf{Ir}^{V}(O^{\bullet})(OH)_2{}^+$ to $\mathbf{Ir}^{V}(O^{\bullet})_2(OH)^+$. Catalytic water oxidation driven by stoichiometric amounts of CAN show a first-order dependence on CAN.[18–19] When periodate was used as oxidant, a half-order dependence on periodate was observed.[19] Since periodate is a two-electron oxidant[24] these data also point to a one-electron oxidation process taking part in the rate-limiting step.

Since the formation of $\mathbf{Ir}^{V}(=O)(O^{\bullet})^+$ is relatively easy, one might expect that the rate-limiting one-electron oxidation must be ascribed to oxidation of $\mathbf{Ir}^{V}(=O)(O^{\bullet})^+$ to $\mathbf{Ir}^{V}(O^{\bullet})_2(OH)^+$. To get the big picture of how this takes place we had to calibrate the energy of the first PCET step, $\mathbf{Ir}^{III}(OH)^+$ to $\mathbf{Ir}^{IV}(=O)^+$, which we used as reference in Table 1, using the experimental data. Oxidation of water with stoichiometric amounts of CAN is energetically favoured by 43.2 kcal mol^{-1} (E^0(water) = 1.23 V vs. NHE; E^0(CAN) = 1.5–1.7 vs. NHE[25]). From our calculations, if we consider the reverse formation of $\mathbf{Ir}^{V}(O^{\bullet})_2(OH)^+$ from $\mathbf{Ir}^{III}(OH)^+$ by coordination of O_2 to $\mathbf{Ir}^{III}(OH)$ and subsequent O–O bond scission, we have a reaction with an energy demand of 30.3 kcal mol^{-1} (6.5 from the reverse reaction of Figure 4 and 23.8 from the reaction of Scheme 6). Consequently, the formation of $\mathbf{Ir}^{V}(O^{\bullet})_2(OH)^+$ is an energetically favoured reaction upon oxidation of $\mathbf{Ir}^{III}(OH)^+$ with four equivalents of CAN, for which 12.9 kcal mol^{-1} was found. This value is the total energy demand of the following steps: $\mathbf{Ir}^{III}(OH)^+ \rightarrow \mathbf{Ir}^{IV}(=O)^+ \rightarrow \mathbf{Ir}^{IV}(OH)_2{}^+ \rightarrow \mathbf{Ir}^{V}(=O)(OH)^+ \rightarrow \mathbf{Ir}^{V}(OH)_3{}^+ \rightarrow \mathbf{Ir}^{V}(O^{\bullet})(OH)_2{}^+ \rightarrow \mathbf{Ir}^{V}(O^{\bullet})_2(OH)^+$.

By using Tables 1 and 2 it is possible to calculate the value for the $\mathbf{Ir}^{III}(OH)^+ \rightarrow \mathbf{Ir}^{IV}(=O)^+$ step, which was found to be 12.4 kcal mol^{-1}. This calculation can be described in a more formal manner by Equation (4)

$$x = 2.39 \times 10^{-4} F\left(E^0_{WO} - E^0_{CAN}\right) + \left(\frac{\sum SE + \sum \Delta\Delta G_{298} + 30.3}{4}\right) \quad (4)$$

where x is the energy of the standard oxidation reaction of $\mathbf{Ir}^{III}(OH)^+$ to $\mathbf{Ir}^{IV}(=O)^+$ (Table 1), F the Faraday constant, E^0_{CAN} the cell potential of the Ce^{IV}/Ce^{III} couple, E^0_{WO} the standard potential of water oxidation and ΣSE and $\Sigma\Delta\Delta G_{298}$ are the sums of individual PCET and water-addition steps required to undergo one catalytic cycle (see Tables 1 and 2). The term 2.39×10^{-4} converts from joules to kilocalories per mole, and 30.3 is the energy difference between $\mathbf{Ir}^{V}(O^{\bullet})_2(OH)^+$ and $\mathbf{Ir}^{III}(OH)^+$ in kilocalories per mole. This shows that oxidation of $\mathbf{Ir}^{III}(OH)^+$ with 1 M CAN is exothermic by 12.4 kcal mol^{-1}. The potential-energy diagram depicted in Figure 5 shows that the first three PCET reactions are exothermic and produce $\mathbf{Ir}^{V}(=O)(O^{\bullet})^+$, which must be the calculated energy minimum for a large excess of oxidant. The last PCET reaction is endothermic and contributes to the rate law of the water-oxidation reaction. This fits with a first-order dependence on equivalents of a one-electron oxidant. The rate-limiting step is formation of the O–O bond, which proceeds over an effective barrier of 24.6 kcal mol^{-1} via $\mathbf{Ir}^{V}(O^{\bullet})(OH)_2{}^+$ and $\mathbf{Ir}^{V}(O^{\bullet})_2(OH)^+$. This barrier is significantly lower than that of O–O bond formation starting from $\mathbf{Ir}^{IV}(=O)^+$, $\mathbf{Ir}^{V}(=O)(OH)^+$, $\mathbf{Ir}^{V}(=O)(O^{\bullet})^+$ and $\mathbf{Ir}^{V}(O^{\bullet})(OH)^{2+}$ intermediates. Consequently, it seems unlikely that O–O bond formation under strongly oxidative conditions can occur via intermediates in which iridium has a low formal oxidation state. The mechanism depicted in Figure 5 describes the key O–O bond-formation and O_2-release steps. It is difficult to exclude that part of the catalytic cycle proceeds via neutral or dicationic intermediates, but so far O–O bond-formation energies seem to indicate that formation of the O–O bond in monocationic systems is more successful. It is remarkable that four sequential oxidation steps occur relatively smoothly to give an intermediate that has a formal Ir^{VII} oxidation state. Here the strongly electron donating character of the ligands and the flexibility of the complex in accommodating different coordination geometries and expanding its coordination sphere with additional aqua ligands during the sequential oxidation steps are of key importance. Expansion of the coordination sphere during water oxidation is not unprecedented and was successfully employed by Sun et al. to obtain very active ruthenium-based water-oxidation catalysts.[26]

Equation (4) can be used to calculate the PES at any given potential, simply by replacing E^0_{CAN} with the redox potential of the oxidant or an externally applied potential of choice (see Figure 6). The results show that at very low concentrations of CAN, or at potentials lower than 1.7 V, it is more difficult to attain the higher-oxidation-state iridium species because the PCET steps become less energetically favourable. Under these conditions O–O bond formation via $Ir^{V}(O^{\bullet})_2(OH)^+$ will be in competition with intramolecular O–O bond formation at $Ir^{V}(=O)(O^{\bullet})^+$ (see Figure 3). For this latter pathway a zero-order dependence in oxidant is expected, as $Ir^{V}(=O)(O^{\bullet})^+$ is the calculated energy minimum at potentials slightly above 1.23 V. Even at the lowest CAN concentrations tested (1 mM,) a first-order rate dependence in oxidizing equivalents was observed; hence, this pathway does not seem to be important under the conditions tested.

The PES depicted in Figure 6 also shows the pitfall of the flexibility of the iridium catalyst. The PES at 1.7 V versus NHE, suggests that $\mathbf{Ir}^{V}(=O)(O^{\bullet})^+$ is the calculated energy minimum of the reaction.[21] If its formation could be avoided and the $\mathbf{Ir}^{V}(O^{\bullet})_2(OH)^+$ species were directly obtained from $\mathbf{Ir}^{V}(OH)_3{}^+$, this would significantly reduce the overall barrier for O–O bond formation. The presented DFT calculations in combination with observation of some of the proposed catalytic intermediates by in situ mass spectroscopy suggest that **Ir** itself could be the active species in catalytic water oxidation. It is difficult to predict the extent to which catalytic water oxidation by **Ir** occurs prior to loss of the Cp* ligand. Previous reports appear contradictory or at least suggest that Cp* loss heavily depends on the catalytic conditions employed.[16,17] Electro-

© 2014 Wiley-VCH Verlag GmbH & Co. KGaA, Weinheim

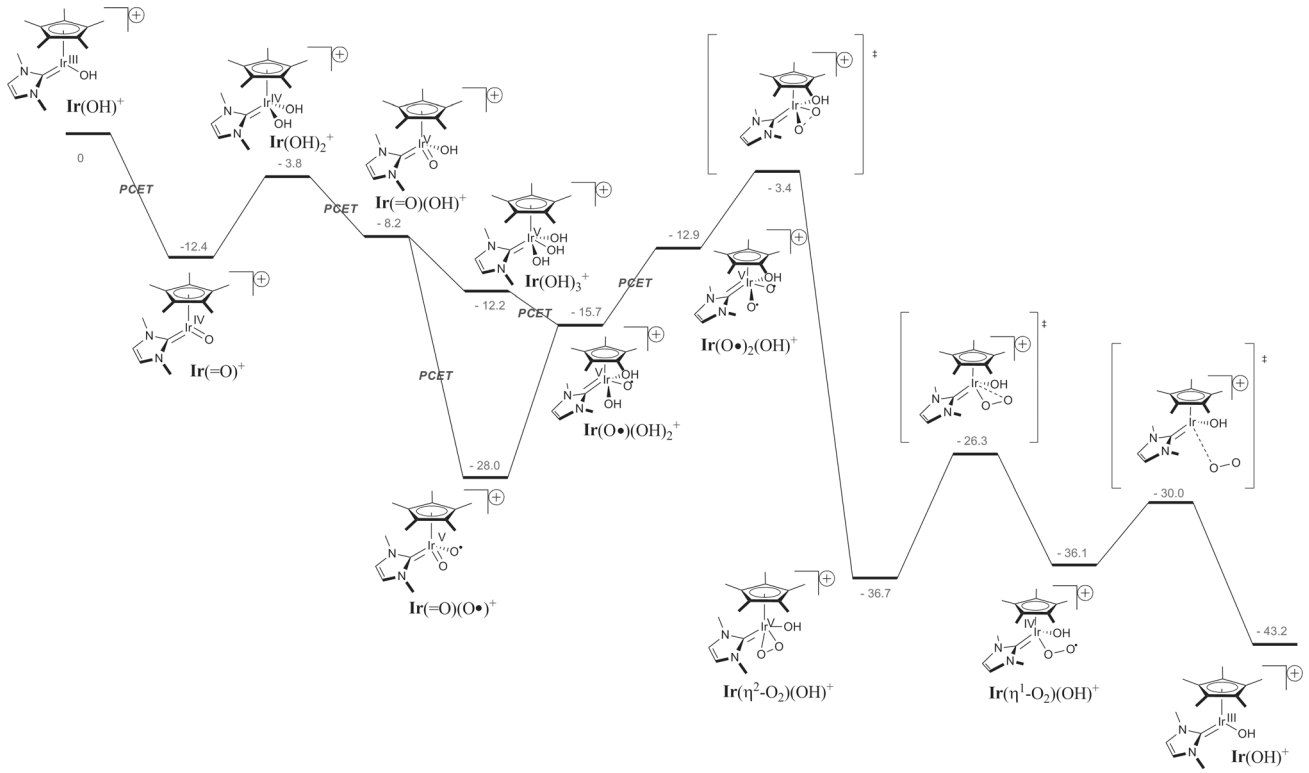

Figure 5. Potential-energy landscape of the water-oxidation reaction catalysed by **Ir**$(OH)^+$. Qualitative values were obtained by DFT calculations and correlated to the PCET reaction between $\mathbf{Ir}^{III}(OH)^+$ and $\mathbf{Ir}^{IV}(=O)^+$. The energy of this PCET step was estimated from the thermodynamic parameters of CAN-driven water oxidation under standard conditions (pH 0, 1 M CAN) according to Equation (4). Changing the potential at which catalysis occurs, either by shifting the concentration in oxidant or by applying a different external potential, results in simultaneous shifts of all PCET steps.

chemical studies to pinpoint the integrity and longevity of the Cp* unit in the case of **Ir**$(OH)_2$ are currently in progress.

Conclusion

The various reaction channels possible for water oxidation with the molecular iridium complexes studied here compete with each other, and our theoretical calculations show that the applied potential favours certain channels. Our results support a mechanism for catalytic water oxidation under harsh oxidative conditions mediated by $[IrCp^*(Me_2NHC)(OH)_2]$. Water-oxidation catalysis occurs by four sequential oxidation steps prior to formation of the O–O bond. In the catalytic mechanism $\mathbf{Ir}^V(=O)(O^\bullet)^+$ is the calculated energy minimum and formation of the O–O bond is rate-limiting. Formation of the O–O bond occurs by intramolecular coupling of two oxo ligands, which is in sharp contrast to a related ruthenium system reported earlier, for which such a pathway proved to be impossible.[20a]

The calculated pathway is in line with previously reported kinetics studies and in situ detection of the lower-oxidation-state catalytic intermediates by mass spectrometry,[18] although the experimental conditions necessary for the MS experiments have not allowed us so far to detect high-oxidation-state intermediates such as $\mathbf{Ir}^V(=O)(O^\bullet)^+$.[21] The mechanism differs greatly from that of other iridium-based water-oxidation catalysts in which water oxidation occurs via nucleophilic attack of water on an Ir^V oxo species. In the case of $[IrCp^*(Me_2NHC)(OH)_2]$, instead of a very reactive Ir^V oxo species, a stable Ir^V trihydroxide species is formed, which does not allow for O–O bond formation at an early stage of the catalytic cycle. Due to coordination of additional aqua ligands in combination with strongly electron donating ligands, further PECT steps are accessible. This shows the potential of catalytic systems that allow for expansion of the coordination sphere during the oxidation sequence, which may be an excellent tool to prevent scaling relationships, from which heterogeneous systems tend to suffer.[27] In the case of molecular ruthenium catalysts, expansion of the coordination number during catalytic water oxidation has previously led to some of the most active water-oxidation catalysts reported thus far.[11]

Experimental Section

We examined nine of the sets of iridium intermediates and seven of the sets of the corresponding water-coordinated complexes that make up the whole reaction (see Scheme 1). DFT calculations were carried out with the Truhlar M06 hybrid functional,[28] together with the 6-311 + G(d,p) basis set for C, N, O and H and the Stuttgart/Cologne small-core relativistic energy-consistent ECP with their correlation-consistent basis sets of double-ζ quality for the 5d transition metal Ir (ECP60MDF/VDZ basis set)[29] within the framework of the Gaussian 09 suite of programs.[30] The peculiarity of these pseudopotentials is that they incorporate both scalar and spin–orbit relativistic effects and are expected to be more appropriate to describe transition metals. All the molecular structures

© 2014 Wiley-VCH Verlag GmbH & Co. KGaA, Weinheim

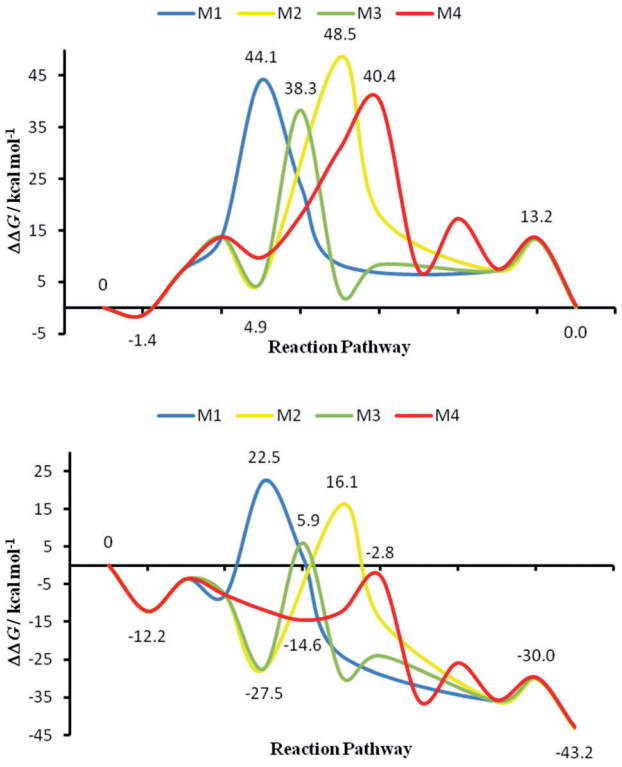

Figure 6. PES at 1.23 V versus NHE (top) and at 1.7 V versus NHE (bottom). M1: O–O bond formation occurs via addition of water to $\mathbf{Ir}^{V}(=O)(OH)$; M2: O–O bond formation occurs via addition of water to $\mathbf{Ir}^{V}(=O)(O^{\bullet})$; M3: O–O bond formation occurs via direct O–O bond formation in $\mathbf{Ir}^{V}(=O)(O^{\bullet})^{+}$; M4: O–O bond formation occurs via direct O–O bond formation in $\mathbf{Ir}^{V}(OH)(O^{\bullet})_2^{+}$. Other mechanisms are not depicted for the sake of clarity, because the found barriers were too high to be relevant. The PES diagram shows that at 1.23 V (top) formation of O_2 is difficult and that the M1, M3 and M4 pathways are in competition with each other, whereby direct O–O coupling at $\mathbf{Ir}^{V}(=O)(O^{\bullet})^{+}$ (M3) prevails. At 1.7 V versus NHE (bottom) formation of the high-oxidation-state iridium complexes is much more favourable, and consequently formation of $\mathbf{Ir}^{V}(O^{\bullet})_2(OH)^{+}$ is possible and O–O bond formation at this species is facile (M4).

were fully optimized by using the CPCM continuum model (water)[31] and the Berny analytical gradient optimization method, whereby the stationary points were characterized by frequency calculation. The intrinsic reaction coordinate (IRC) was used to trace the path of the chemical reactions. Thermochemical analysis (free energies $\Delta\Delta G$) was performed at 298.15 K, starting from the frequency calculations.

Acknowledgements

This work has been financed by the Italian National Research Council (CNR, "SolarFuelTandem") and the Netherlands Organization of Scientific Research (NWO-CW) within the EUROCORES Programme EuroSolarFuels of the European Science Foundation (ESF). D.H. thanks the Netherlands Organization of Scientific Research (NWO-CW, VENI grant 700.59.410) and A.V. and A.B. thank the CNR project PM.P04.010 (MACOL) and the "Progetto Bandiera" N-CHEM.

Keywords: density functional calculations · iridium · oxidation · reaction mechanisms · water splitting

[1] a) N. S. Lewis, D. G. Nocera, *Proc. Natl. Acad. Sci. USA* **2006**, *103*, 15729–15735; b) R. E. Blankenship, D. M. Tiede, J. Barber, G. W. Brudvig, G. Fleming, M. Ghirardi, M. R. Gunner, W. Junge, D. M. Kramer, A. Melis, T. A. Moore, C. C. Moser, D. G. Nocera, A. J. Nozik, D. R. Ort, W. W. Parson, R. C. Prince, R. T. Sayre, *Science* **2011**, *332*, 805–809; c) N. D. McDaniel, S. Bernhard, *Dalton Trans.* **2010**, *39*, 10021–10030; d) K. J. Young, L. A. Martini, R. L. Milot, R. C. Snoeberger, V. S. Batista, C. A. Schmuttenmaer, R. H. Crabtree, G. W. Brudvig, *Coord. Chem. Rev.* **2012**, *256*, 2503–2520; e) D. G. H. Hetterscheid, J. I. van der Vlugt, B. de Bruin, J. N. H. Reek, *Angew. Chem.* **2009**, *121*, 8324–8327; *Angew. Chem. Int. Ed.* **2009**, *48*, 8178–8181.

[2] a) N. Armaroli, V. Balzani, *Energy for a Sustainable World: From the Oil Age to a Sun-Powered Future*, Wiley-VCH, Weinheim, **2011**, p. xxi, p. 368; b) N. Armaroli, V. Balzani, *Angew. Chem.* **2007**, *119*, 52–67; *Angew. Chem. Int. Ed.* **2007**, *46*, 52–66.

[3] S. W. Gersten, G. J. Samuels, T. J. Meyer, *J. Am. Chem. Soc.* **1982**, *104*, 4029–4030.

[4] a) J. J. Concepcion, M. K. Tsai, J. T. Muckerman, T. J. Meyer, *J. Am. Chem. Soc.* **2010**, *132*, 1545–1557; b) J. J. Concepcion, J. W. Jurss, M. R. Norris, Z. F. Chen, J. L. Templeton, T. J. Meyer, *Inorg. Chem.* **2010**, *49*, 1277–1279; c) D. J. Wasylenko, C. Ganesamoorthy, M. A. Henderson, B. D. Koivisto, H. D. Osthoff, C. P. Berlinguette, *J. Am. Chem. Soc.* **2010**, *132*, 16094–16106; d) H. W. Tseng, R. Zong, J. T. Muckerman, R. Thummel, *Inorg. Chem.* **2008**, *47*, 11763–11773; e) D. J. Wasylenko, R. D. Palmer, C. P. Berlinguette, *Chem. Commun.* **2013**, *49*, 218–227; f) D. G. H. Hetterscheid, J. N. H. Reek, *Angew. Chem.* **2012**, *124*, 9878–9885; *Angew. Chem. Int. Ed.* **2012**, *51*, 9740–9747; g) R. Cao, W. Z. Lai, P. W. Du, *Energy Environ. Sci.* **2012**, *5*, 8134–8157.

[5] a) M. W. Kanan, Y. Surendranath, D. G. Nocera, *Chem. Soc. Rev.* **2009**, *38*, 109–114; b) M. W. Kanan, D. G. Nocera, *Science* **2008**, *321*, 1072–1075.

[6] a) J. Limburg, J. S. Vrettos, L. M. Liable-Sands, A. L. Rheingold, R. H. Crabtree, G. W. Brudvig, *Science* **1999**, *283*, 1524–1527; b) G. C. Dismukes, R. Brimblecombe, G. A. N. Felton, R. S. Pryadun, J. E. Sheats, L. Spiccia, G. F. Swiegers, *Acc. Chem. Res.* **2009**, *42*, 1935–1943; c) N. S. McCool, D. M. Robinson, J. E. Sheats, G. C. Dismukes, *J. Am. Chem. Soc.* **2011**, *133*, 11446–11449.

[7] a) J. L. Fillol, Z. Codola, I. Garcia-Bosch, L. Gomez, J. J. Pla, M. Costas, *Nat. Chem.* **2011**, *3*, 807–813; b) W. C. Ellis, N. D. McDaniel, S. Bernhard, T. J. Collins, *J. Am. Chem. Soc.* **2010**, *132*, 10990–10991.

[8] a) D. J. Wasylenko, R. D. Palmer, E. Schott, C. P. Berlinguette, *Chem. Commun.* **2012**, *48*, 2107–2109; b) Q. S. Yin, J. M. Tan, C. Besson, Y. V. Geletii, D. G. Musaev, A. E. Kuznetsov, Z. Luo, K. I. Hardcastle, C. L. Hill, *Science* **2010**, *328*, 342–345; c) D. K. Dogutan, R. McGuire, D. G. Nocera, *J. Am. Chem. Soc.* **2011**, *133*, 9178–9180; d) G. B. Zhu, Y. V. Geletii, P. Kogerler, H. Schilder, J. Song, S. Lense, C. C. Zhao, K. I. Hardcastle, D. G. Musaev, C. L. Hill, *Dalton Trans.* **2012**, *41*, 2084–2090.

[9] a) S. M. Barnett, K. I. Goldberg, J. M. Mayer, *Nat. Chem.* **2012**, *4*, 498–502; b) Z. F. Chen, T. J. Meyer, *Angew. Chem.* **2013**, *125*, 728–731; *Angew. Chem. Int. Ed.* **2013**, *52*, 700–703.

[10] a) A. Petronilho, M. Rahman, J. A. Woods, H. Al-Sayyed, H. Muller-Bunz, J. M. D. MacElroy, S. Bernhard, M. Albrecht, *Dalton Trans.* **2012**, *41*, 13074–13080; b) R. Lalrempuia, N. D. McDaniel, H. Muller-Bunz, S. Bernhard, M. Albrecht, *Angew. Chem.* **2010**, *122*, 9959–9962; *Angew. Chem. Int. Ed.* **2010**, *49*, 9765–9768; c) A. Savini, G. Bellachioma, G. Ciancaleoni, C. Zuccaccia, D. Zuccaccia, A. Macchioni, *Chem. Commun.* **2010**, *46*, 9218–9219; d) C. Y. Lee, S. X. Guo, A. F. Murphy, T. McCormac, J. Zhang, A. M. Bond, G. B. Zhu, C. L. Hill, Y. V. Geletii, *Inorg. Chem.* **2012**, *51*, 11521–11532; e) L. P. Tong, A. K. Inge, L. L. Duan, L. Wang, X. D. Zou, L. C. Sun, *Inorg. Chem.* **2013**, *52*, 2505–2518; f) L. P. Tong, Y. Wang, L. L. Duan, Y. H. Xu, X. Cheng, A. Fischer, M. S. G. Ahlquist, L. C. Sun, *Inorg. Chem.* **2012**, *51*, 3388–3398; g) Y. H. Xu, A. Fischer, L. L. Duan, L. P. Tong, E. Gabrielsson, B. Akermark, L. C. Sun, *Angew. Chem.* **2010**, *122*, 9118–9121; *Angew. Chem. Int. Ed.* **2010**, *49*, 8934–8937; h) L. L. Duan, A. Fischer, Y. H. Xu, L. C. Sun, *J. Am. Chem. Soc.* **2009**, *131*, 10397–10399; i) Y. H. Xu, T. Akermark, V. Gyollai, D. P. Zou, L. Eriksson, L. L. Duan, R. Zhang, B. Akermark, L. C. Sun, *Inorg. Chem.* **2009**, *48*, 2717–2719; j) L. Wang, L. L.

© 2014 Wiley-VCH Verlag GmbH & Co. KGaA, Weinheim

Duan, B. Stewart, M. P. Pu, J. H. Liu, T. Privalov, L. C. Sun, *J. Am. Chem. Soc.* **2012**, *134*, 18868 – 18880; k) D. Moonshiram, I. Alperovich, J. J. Concepcion, T. J. Meyer, Y. Pushkar, *Proc. Natl. Acad. Sci. USA* **2013**, *110*, 3765 – 3770; l) C. J. Gagliardi, A. K. Vannucci, J. J. Concepcion, Z. F. Chen, T. J. Meyer, *Energy Environ. Sci.* **2012**, *5*, 7704 – 7717; m) J. J. Concepcion, J. W. Jurss, J. L. Templeton, T. J. Meyer, *Proc. Natl. Acad. Sci. USA* **2008**, *105*, 17632 – 17635; n) S. Maji, I. Lopez, F. Bozoglian, J. Benet-Buchholz, A. Llobet, *Inorg. Chem.* **2013**, *52*, 3591 – 3593; o) A. Bucci, A. Savini, L. Rocchigiani, C. Zuccaccia, S. Rizzato, A. Albinati, A. Llobet, A. Macchioni, *Organometallics* **2012**, *31*, 8071 – 8074; p) S. Maji, L. Vigara, F. Cottone, F. Bozoglian, J. Benet-Buchholz, A. Llobet, *Angew. Chem.* **2012**, *124*, 6069 – 6072; *Angew. Chem. Int. Ed.* **2012**, *51*, 5967 – 5970; q) L. Francas, X. Sala, E. Escudero-Adan, J. Benet-Buchholz, L. Escriche, A. Llobet, *Inorg. Chem.* **2011**, *50*, 2771 – 2781; r) F. Bozoglian, S. Romain, M. Z. Ertem, T. K. Todorova, C. Sens, J. Mola, M. Rodriguez, I. Romero, J. Benet-Buchholz, X. Fontrodona, C. J. Cramer, L. Gagliardi, A. Llobet, *J. Am. Chem. Soc.* **2009**, *131*, 15176 – 15187; s) D. E. Polyansky, J. T. Muckerman, J. Rochford, R. F. Zong, R. P. Thummel, E. Fujita, *J. Am. Chem. Soc.* **2011**, *133*, 14649 – 14665.

[11] L. Duan, F. Bozoglian, S. Mandal, B. Stewart, T. Privalov, A. Llobet, L. Sun, *Nat. Chem.* **2012**, *4*, 418 – 423.

[12] N. D. McDaniel, F. J. Coughlin, L. L. Tinker, S. Bernhard, *J. Am. Chem. Soc.* **2008**, *130*, 210 – 217.

[13] a) J. D. Blakemore, N. D. Schley, D. Balcells, J. F. Hull, G. W. Olack, C. D. Incarvito, O. Eisenstein, G. W. Brudvig, R. H. Crabtree, *J Am Chem. Soc* **2010**, *132*, 16017 – 16029; b) J. Graeupner, T. P. Brewster, J. D. Blakemore, N. D. Schley, J. M. Thomsen, G. W. Brudvig, N. Hazari, R. H. Crabtree, *Organometallics* **2012**, *31*, 7158 – 7164; c) M. Zhou, U. Hintermair, B. G. Hashiguchi, A. R. Parent, S. M. Hashmi, M. Elimelech, R. A. Periana, G. W. Brudvig, R. H. Crabtree, *Organometallics* **2013**, *32*, 957 – 965; d) T. P. Brewster, J. D. Blakemore, N. D. Schley, C. D. Incarvito, N. Hazari, G. W. Brudvig, R. H. Crabtree, *Organometallics* **2011**, *30*, 965 – 973; e) J. F. Hull, D. Balcells, J. D. Blakemore, C. D. Incarvito, O. Eisenstein, G. W. Brudvig, R. H. Crabtree, *J. Am. Chem. Soc.* **2009**, *131*, 8730 – 8731.

[14] a) A. Savini, P. Belanzoni, G. Bellachioma, C. Zuccaccia, D. Zuccaccia, A. Macchioni, *Green Chem.* **2011**, *13*, 3360 – 3374; b) C. Zuccaccia, G. Bellachioma, S. Bolano, L. Rocchigiani, A. Savini, A. Macchioni, *Eur. J. Inorg. Chem.* **2012**, 1462 – 1468.

[15] a) U. Hintermair, S. M. Hashmi, M. Elimelech, R. H. Crabtree, *J. Am. Chem. Soc.* **2012**, *134*, 9785 – 9795; b) H. Junge, N. Marquet, A. Kammer, S. Denurra, M. Bauer, S. Wohlrab, F. Gartner, M. M. Pohl, A. Spannenberg, S. Gladiali, M. Beller, *Chem. Eur. J.* **2012**, *18*, 12749 – 12758.

[16] U. Hintermair, S. W. Sheehan, A. R. Parent, D. H. Ess, D. T. Richens, P. H. Vaccaro, G. W. Brudvig, R. H. Crabtree, *J. Am. Chem. Soc.* **2013**, *135*, 10837 – 10851.

[17] K. S. Joya, N. K. Subbaiyan, F. D'Souza, H. J. M. de Groot, *Angew. Chem.* **2012**, *124*, 9739 – 9743; *Angew. Chem. Int. Ed.* **2012**, *51*, 9601 – 9605.

[18] D. G. H. Hetterscheid, J. N. H. Reek, *Chem. Commun.* **2011**, *47*, 2712 – 2714.

[19] D. G. H. Hetterscheid, J. N. H. Reek, *Eur. J. Inorg. Chem.* **2014**, 742.

[20] a) X. Sala, M. Z. Ertem, L. Vigara, T. K. Todorova, W. Z. Chen, R. C. Rocha, F. Aquilante, C. J. Cramer, L. Gagliardi, A. Llobet, *Angew. Chem.* **2010**, *122*, 7911 – 7913; *Angew. Chem. Int. Ed.* **2010**, *49*, 7745 – 7747; b) L. Vilella, P. Vidossich, D. Balcells, A. Lledos, *Dalton Trans.* **2011**, *40*, 11241 – 11247.

[21] The mass-spectrometric experiments described in a previous communication[18] were carried out at very low concentrations of catalyst and CAN. Consequently, the concentration of CAN employed under mass-spectrometric conditions (≈1 μM) was roughly 4–5 orders of magnitudes lower than the CAN concentrations used in our catalytic experiments (10–300 mM). Under these dilute conditions and in the absence of an acid (pH > 5), CAN is not very stable and is prone to form a cerium oxide. Due to the instability of CAN and potential side reactions of CAN with impurities in the mass spectrometer, it is difficult to observe the higher-oxidation-state species under these conditions. Moreover, since formation of these species will be slow, possible side reactions independent of the CAN concentration may become important. These include reduction of the catalytic species by impurities present in the mass spectrometer, release of reactive oxygen species and decomposition of the catalysts. The fact that $\mathbf{Ir}^{V}(=O)(O^{\bullet})^{+}$ has not yet been detected under these non-catalytic mass-spectrometric conditions does not rule out involvement of this species in the catalytic cycle.

[22] a) E. Poverenov, I. Efremenko, A. I. Frenkel, Y. Ben-David, L. J. W. Shimon, G. Leitus, L. Konstantinovski, J. M. L. Martin, D. Milstein, *Nature* **2008**, *455*, 1093 – 1096; b) B. G. Jacobi, D. S. Laitar, L. H. Pu, M. F. Wargocki, A. G. DiPasquale, K. C. Fortner, S. M. Schuck, S. N. Brown, *Inorg. Chem.* **2002**, *41*, 4815 – 4823; c) K. C. Fortner, D. S. Laitar, J. Muldoon, L. H. Pu, S. B. Braun-Sand, O. Wiest, S. N. Brown, *J. Am. Chem. Soc.* **2007**, *129*, 588 – 600.

[23] X. Sala, I. Romero, M. Rodriguez, L. Escriche, A. Llobet, *Angew. Chem.* **2009**, *121*, 2882 – 2893; *Angew. Chem. Int. Ed.* **2009**, *48*, 2842 – 2852.

[24] A. R. Parent, T. P. Brewster, W. De Wolf, R. H. Crabtree, G. W. Brudvig, *Inorg. Chem.* **2012**, *51*, 6147 – 6152.

[25] Potentials of CAN between 1.5 and 1.7 have been reported. Since the catalysis data were obtained under pseudo-zero-order conditions, the redox strength of CAN is relatively high compared to the potentials of the catalyst according to the Nernst law. We therefore chose to work with 1.7 V versus NHE.

[26] J. Nyhlén, L. L. Duan, B. Akermark, L. C. Sun, T. Privalov, *Angew. Chem.* **2010**, *122*, 1817 – 1821; *Angew. Chem. Int. Ed.* **2010**, *49*, 1773 – 1777.

[27] M. T. M. Koper, *Chem. Sci.* **2013**, *4*, 2710 – 2723.

[28] Y. Zhao, N. E. Schultz, D. G. Truhlar, *J. Chem. Theory Comput.* **2006**, *2*, 364 – 382.

[29] D. Figgen, K. A. Peterson, M. Dolg, H. Stoll, *J. Chem. Phys.* **2009**, *130*, 164108.

[30] Gaussian 09, Revision A.02, M. J. Frisch, G. W. Trucks, H. B. Schlegel, G. E. Scuseria, M. A. Robb, J. R. Cheeseman, G. Scalmani, V. Barone, B. Mennucci, G. A. Petersson, H. Nakatsuji, M. Caricato, X. Li, H. P. Hratchian, A. F. Izmaylov, J. Bloino, G. Zheng, J. L. Sonnenberg, M. Hada, M. Ehara, K. Toyota, R. Fukuda, J. Hasegawa, M. Ishida, T. Nakajima, Y. Honda, O. Kitao, H. Nakai, T. Vreven, J. A. Montgomery, Jr., J. E. Peralta, F. Ogliaro, M. Bearpark, J. J. Heyd, E. Brothers, K. N. Kudin, V. N. Staroverov, R. Kobayashi, J. Normand, K. Raghavachari, A. Rendell, J. C. Burant, S. S. Iyengar, J. Tomasi, M. Cossi, N. Rega, J. M. Millam, M. Klene, J. E. Knox, J. B. Cross, V. Bakken, C. Adamo, J. Jaramillo, R. Gomperts, R. E. Stratmann, O. Yazyev, A. J. Austin, R. Cammi, C. Pomelli, J. W. Ochterski, R. L. Martin, K. Morokuma, V. G. Zakrzewski, G. A. Voth, P. Salvador, J. J. Dannenberg, S. Dapprich, A. D. Daniels, Ö. Farkas, J. B. Foresman, J. V. Ortiz, J. Cioslowski, D. J. Fox, Gaussian, Inc., Wallingford CT, **2009**.

[31] M. Cossi, N. Rega, G. Scalmani, V. Barone, *J. Comput. Chem.* **2003**, *24*, 669 – 681.

Received: September 27, 2013
Revised: January 8, 2014
Published online on March 18, 2014

© 2014 Wiley-VCH Verlag GmbH & Co. KGaA, Weinheim